◆ Human Brain Mapping 9:81–92(2000) ◆

Mathematical/Computational Challenges in Creating Deformable and Probabilistic Atlases of the Human Brain

Paul M. Thompson,[1]* Roger P. Woods,[1] Michael S. Mega,[1,2] and Arthur W. Toga

[1]*Laboratory of Neuro Imaging, Department of Neurology, Division of Brain Mapping, UCLA School of Medicine, Los Angeles, California* [2]*Alzheimer's Disease Center, UCLA School of Medicine, Los Angeles, California*

Abstract: Striking variations in brain structure, especially in the gyral patterns of the human cortex, present fundamental challenges in human brain mapping. Probabilistic brain atlases, which encode information on structural and functional variability in large human populations, are powerful research tools with broad applications. Knowledge-based imaging algorithms can also leverage atlased information on anatomic variation. Applications include automated image labeling, pathology detection in individuals or groups, and investigating how regional anatomy is altered in disease, and with age, gender, handedness and other clinical or genetic factors. In this report, we illustrate some of the mathematical challenges involved in constructing population-based brain atlases. A *disease-specific atlas* is constructed to represent the human brain in Alzheimer's disease (AD). Specialized strategies are developed for population-based averaging of anatomy. Sets of high-dimensional elastic mappings, based on the principles of continuum mechanics, reconfigure the anatomy of a large number of subjects in an anatomic image database. These mappings generate a local encoding of anatomic variability and are used to create a crisp anatomical image template with highly resolved structures in their mean spatial location. Specialized approaches are also developed to average cortical topography. Since cortical patterns are altered in a variety of diseases, gyral pattern matching is used to encode the magnitude and principal directions of local cortical variation. In the resulting cortical templates, subtle features emerge. Regional asymmetries appear that are not apparent in individual anatomies. Population-based maps of cortical variation reveal a mosaic of variability patterns that segregate sharply according to functional specialization and cytoarchitectonic boundaries. *Hum. Brain Mapping 9:81–92, 2000.*

Key words: brain mapping; brain atlases; cerebral cortex; morphometry; Alzheimer's disease

This report was presented at the Proceedings of the 1998 Brain Map Conference, San Antonio, TX. Contract grant sponsor: NIMH and NIDA, Human Brain Project grant to the International Consortium for Brain Mapping; Contract grant number: P20 MH/DA52176; Contract grant sponsor, NCRR, P41 Resource Grant (to P.T., R.P.W, A.W.T.); Contract grant sponsor: United States Information Agency; Contract grant number: G-1-00001; Contract grant sponsor: Howard Hughes Medical Institute (to P.T.); Contract sponsor: U.S.-U.K. Fulbright Commission, London (to P.T.); Contract grant sponsor: NINCDS (to R.P.W.); Contract grant number: K08-NS01646; Contract grant sponsor: NIA (to M.S.M.); Contract grant number: K08-AG100784; Contract grant sponsor: National Library of Medicine (to A.W.T.); Contract grant number: LM/MH05639; Contract grant sponsor: National Science Foundation (to A.W.T.); Contract grant number: BIR 93-22434; Contract grant sponsor: NCRR (to A.W.T.); Congtract grant number: RR05956; Contract grant sponsor: NINCDS/NIMH (to A.W.T.); Contract grant number: NS38753.

*Correspondence to: Dr. Paul Thompson, Rm 4238, Reed Neurological Research Center, Laboratory of Neuro Imaging, Department of Neurology, UCLA School of Medicine, 710 Westwood Plaza, Los Angeles, CA 90095-1769. E-mail thompson@loni.ucla.edu

Received for publication 30 March 1999; Accepted 24 September 1999.

INTRODUCTION

Extreme variations in brain structure in human populations present fundamental challenges in human brain mapping. First, wide variations in the gyral patterns of the human cortex make it difficult to integrate data from different subjects. Cortical anatomy is so variable and complex that group-specific patterns are obscured. Research has focused on uncovering specific patterns of anatomic alterations in Alzheimer's disease (AD) or other dementias [Friedland and Luxenberg, 1988], schizophrenia [Kikinis et al., 1994; Csernansky et al., 1998], epilepsy [Cook et al., 1994], attention deficit hyperactivity disorder (ADHD) [Giedd et al., 1994], autism [Filipek et al., 1996; Courchesne, 1997], and cortical dysplasias [Sobire et al., 1995]. To design automated strategies that distinguish abnormalities from normal variants, a realistically complex mathematical framework is required to encode information on anatomic variability in homogeneous populations [Mazziotta et al., 1995; Thompson et al., 1997, 1998; Grenander and Miller, 1998].

Population-based brain atlases

Because there is neither a single representative brain, nor a simple method to construct an "average" anatomy or represent 3D anatomic variations, the construction of brain atlases to represent large human populations has become a research focus [Roland and Zilles, 1994; Fox et al., 1994; Mazziotta et al., 1995; Toga and Thompson, 1999]. *Deformable atlases*, which can be elastically transformed to reflect the anatomy of new subjects, and *probabilistic atlases*, which retain information on population variability, are powerful new research tools with a range of clinical and research applications. These atlases may be used for pathology detection in individuals or groups [Thompson et al., 1997]. They can also guide algorithms for knowledge-based image analysis, automated structure extraction [MacDonald et al., 1998], image labeling [Collins et al., 1994], tissue classification [Zijdenbos and Dawant, 1994], and functional image analysis [Dinov et al., 1999].

Deformable and probabilistic atlases

Due to the complex structural variability among individuals, a fixed brain atlas may not accurately represent every brain [Roland and Zilles, 1994; Mazziotta et al., 1995]. *Deformable brain atlases* are based on the idea that a digital brain atlas can be elastically deformed to fit a new subject's anatomy. Three-dimensional image warping algorithms [see Toga, 1998, for review] can transfer all the information in a digital brain atlas onto the scan of a given subject. Any segment of the atlas anatomy is allowed to grow, shrink, twist, and even rotate, producing an *individualized atlas* that matches the subject in exquisite detail. Such deformable atlases [Seitz et al., 1990; Evans et al., 1991; Christensen et al., 1993; Rizzo et al., 1995; Sandor and Leahy, 1995; Thompson et al., 1997; Gee et al.,1998; Grenander and Miller, 1998] carry 3D maps of functional and vascular territories into subjects' scans, as well as information on tissue types, cytoarchitecture, histologic and neurochemical content [Mega et al., 1997]. As a valuable by-product, 3D warping algorithms also *quantify* local and global shape changes. The complex profiles of dilation and contraction required to warp an atlas onto a new subject's brain provide an index of the anatomical shape differences between that subject's brain and the atlas [Davatzikos et al., 1996; Thompson et al., 1997; Ashburner et al., 1998]. Differences in regional shape can therefore be assessed by the local displacement required to deform one brain volume into another. As a result, deformable atlases not only adapt to individual anatomy, but they offer a powerful strategy to analyze developmental, age-related, or pathologic variations.

Probabilistic atlasing

Probabilistic atlasing [Evans et al., 1994; Mazziotta et al., 1995; Thompson et al., 1996, 1997, 1998] is a research strategy for generating anatomical templates, expert diagnostic systems, and knowledge-based imaging tools that retain quantitative information on intersubject variations in brain architecture. The approach can be applied to analyze functional as well as structural variability [Fox et al., 1994]. Probabilistic atlases of brain *structure* currently fall into three major categories [Thompson and Toga, 1998]. Earlier, *intensity-based* approaches concentrated on generating "average" representations of anatomy by intensity averaging of multiple MRI scans. To facilitate the reporting of brain mapping data in an atlas-based 3D coordinate system, Evans et al. [1994] created a composite MRI dataset from 305 young normal subjects (239 males, 66 females; age: 23.4 $\pm$ 4.1 years) whose scans were linearly mapped into stereotaxic space [Talairach and Tournoux, 1988]. Aligned scans were intensity normalized, and averaged on a voxel-by-voxel basis [*cf.* Ashburner and Friston, 1997]. Automated methods were subsequently developed to align new MRI and

PET data with these digital templates by optimizing a measure of image similarity, such as 3D cross-correlation [Collins et al., 1994, 1995], ratio image uniformity [Woods et al., 1992], squared intensity difference [Woods et al., 1993, 1998; Ashburner et al., 1998], or mutual information [Wells et al., 1997]. Although these templates can be used as targets for automated registration, to map MRI and co-registered functional data into stereotaxic space [Evans et al., 1994], cortical structures are blurred out in the atlas templates due to spatial variability in the population. In *label-based* approaches [Evans et al., 1994], large ensembles of brain data are manually labeled, or tissue-classified, into subvolumes, after mapping individual datasets into stereotaxic space. A probability map is then constructed for each segmented structure by determining the proportion of subjects assigned a given anatomic label at each voxel position in stereotaxic space [Evans et al.,1994; Paus et al., 1996]. Tissue probability maps can be used to assist automated tissue classification [Zijdenbos and Dawant, 1994], radio-frequency inhomogeneity and partial volume correction [Labbe et al., 1996; Sled et al., 1998], and can restrict the search space for significant activations in PET and SPECT imaging experiments [Dinov et al., 1999].

Finally, in *deformation-based* probabilistic atlases [Thompson et al., 1997], a warping algorithm deforms an atlas template into the shape of each brain in a scan database. The amount of deformation required is stored as a 3D map representing local anatomic differences between each subject and the atlas. Statistical properties of these deformation maps are encoded locally to determine the magnitude and directional biases of anatomic variation [Collins et al., 1994; Thompson et al., 1996a,b, 1997, 1998; Davatzikos, 1998]. Methods to compare probabilistic information on brain structure from different subpopulations are under rapid development and include approaches based on random tensor fields [Thompson and Toga, 1997a,b, 1998; Gaser et al., 1998; Thirion et al., 1998; Cao and Worsley, 1999], singular value decomposition and ManCova [Ashburner et al., 1998], shape-theoretic approaches [Bookstein, 1997], stochastic differential equations [Christensen et al., 1993], and pattern theory [Grenander and Miller, 1998]. The resulting atlas systems show promise for encoding patterns of anatomic variation in large image databases, for pathology detection in individuals and groups, and for determining effects on brain structure of age, gender, handedness, and other demographic or genetic factors [Thompson et al., 1999].

Disease-specific atlases

Here, we illustrate some of the mathematical challenges involved in constructing probabilistic brain atlases. A *disease-specific atlas* is constructed to represent the human brain in Alzheimer's disease (AD). Specialized strategies are developed for population-based averaging of anatomy. These approaches treat geometric and intensity variation separately and encode differences in cortical patterns. A set of high-dimensional elastic mappings are calculated, based on the principles of continuum mechanics, matching the anatomy of a large number of subjects in an anatomic database. These mappings generate a local encoding of anatomic variability and are used to create a crisp anatomical image template with highly resolved structures in their mean anatomical configuration. Specialized approaches are also developed to average cortical topography and measure its variation. Since cortical patterns are altered in a variety of diseases, gyral pattern matching is used to encode the local magnitude and principal directions of cortical variation. In the resulting cortical templates, subtle features emerge, along with regional asymmetries that are not apparent in individual anatomies. Maps of cortical variation reveal a mosaic of variability patterns, segregated by functional specialization and cytoarchitectonic boundaries.

METHODS

Subjects

To quantify patterns of anatomic variability in a relatively large, homogeneous group of subjects, a reference image archive was constructed from high-resolution 3D ($256^2 \times 124$) T_1-weighted fast SPGR (spoiled GRASS) MRI volumes, acquired from 26 subjects diagnosed with mild to moderate Alzheimer's disease (AD; NINCDS-ADRDA criteria). All subjects were matched for age (75.8 ± 1.7 yrs.; 14 females/12 males), educational level (15.2 ± 0.4 yr), disease severity, and handedness (all right-handed). The patient group had a mean Mini-Mental State Exam score of 20.0 ± 0.8 (maximum score: 30) [Folstein et al., 1975]. Scan acquisition parameters were TR/TE 14.3/3.2 msec, flip angle 35°, NEX = 1, FOV 25cm, with contiguous 1.5-mm-thick slices (no interslice gap) covering the entire brain.

Cortical modeling

Initially, image data were digitally transformed into a Talairach-based coordinate system that: (1) places

the anterior commissure (AC) at the origin, (2) vertically orients the midsagittal plane, and (3) horizontally orients the AC-PC line. Aligned MR volumes were corrected for nonuniformity of MR signal intensity [Zijdenbos and Dawant, 1994; Sled et al., 1998], and high-resolution surface models of the cerebral cortex were extracted, as described previously [Thompson et al., 1997; MacDonald et al., 1998].

Gyral patterns

Thirty-six major external fissures and sulci in the brain were manually outlined on highly magnified surface-rendered images of each cortical surface. Detailed anatomic criteria were applied as set out in Steinmetz et al. [1990], Leonard et al. [1996], Thompson et al. [1997a,b], and Kennedy et al., [1998] and the sulcal atlas of Ono et al. [1990] to define sulci whose topological consistency has been demonstrated across normal populations. In both hemispheres, 3D curves were drawn to represent superior and inferior frontal, central, postcentral, intraparietal, superior and inferior temporal, collateral, olfactory and occipito-temporal sulci, as well as the Sylvian fissures. Additional 3D curves were drawn in each hemisphere to represent gyral limits at the interhemispheric margin [Thompson et al., 1997]. Stereotaxic locations of contour points derived from the data volume were redigitized to produce 36 uniformly parameterized cortical contours per brain, representing the primary gyral pattern of each subject [Thompson et al., 1997].

Gyral pattern matching, cortical averaging, and variability maps

Due to variations in gyral patterning, cortical variability will be severely underestimated unless elements of the gyral pattern are matched from one subject to another [*cf*. Ge et al., 1994; Collins et al., 1996; Thompson et al., 1996, 1997, 1998; Drury and Van Essen, 1997; Fischl et al., 1999]. This matching is also required for cortical averaging; otherwise, corresponding gyral features will not be averaged together. To find good matches among cortical regions, we perform the matching process in the cortical surface's parametric space, which permits more tractable mathematics (Fig. 1) [Thompson and Toga, 1996, 1998; *cf*. Van Essen and Maunsell, 1980; Sereno et al., 1996; Fischl et al., 1999]. This vector flow field in parametric space indirectly specifies a correspondence field in 3D, which drives one cortical surface into the shape of another. This mapping not only matches overall cortical geometry, but matches the entire network of the 36 landmark curves with their counterparts in the target brain and thus is a valid encoding of cortical variation.

SPHERICAL AND PLANAR MAPS OF THE CORTEX

Computation of an *average* cortical surface is based on the availability of mappings that drive one subject's cortex onto another. These cross-subject mappings are calculated as follows. Because each subject's cortical model is arrived at by deforming a spherical mesh [Davatzikos et al., 1996; Thompson and Toga, 1996], any point on the cortex maps to exactly one point on the sphere, and a *spherical map* of the cortex is made that indexes sulcal landmarks in the normally folded brain surface. These spherical locations, indexed by two parameters, can also be mapped to a plane (Fig. 1) [Thompson et al., 1997; Thompson and Toga, 1998]. Although spherical, or planar, maps involve different amounts of local dilation or contraction of the surface metric, this metric tensor field is stored and used later to adjust the flow that describes the mapping of one cortex onto another. The result is *a covariant regularization* approach (see Appendix) [Einstein, 1914; Thompson and Toga, 1998]. This approach makes it immaterial whether a spherical or planar map is used, since the flows defined on it are adjusted for variations in the metric tensor of the mapping, and the results become independent of the underlying parameterization (spherical or planar).

Retention of 3D cortical information

To ensure that each subject's spherical map can also be converted back into a 3D cortical model, cortical surface point position vectors in 3D stereotaxic space are represented on the sphere using a color-code (at 16 bits per channel). This forms an image of the parameter space in RGB color image format (Fig. 2c,d)[Thompson and Toga, 1997]. To find good matches between cortical regions in different subjects, we first derive a spherical map for each respective surface model and transfer the entire network of sulcal curves back onto it. After performing the matching process using a flow in the spherical parametric space (Fig. 2), the corresponding 3D mapping is recovered, carrying one cortex onto another.

CREATING AN AVERAGE CORTICAL SURFACE

The warping field deforming one cortex into gyral correspondence with another can also be used to cre-

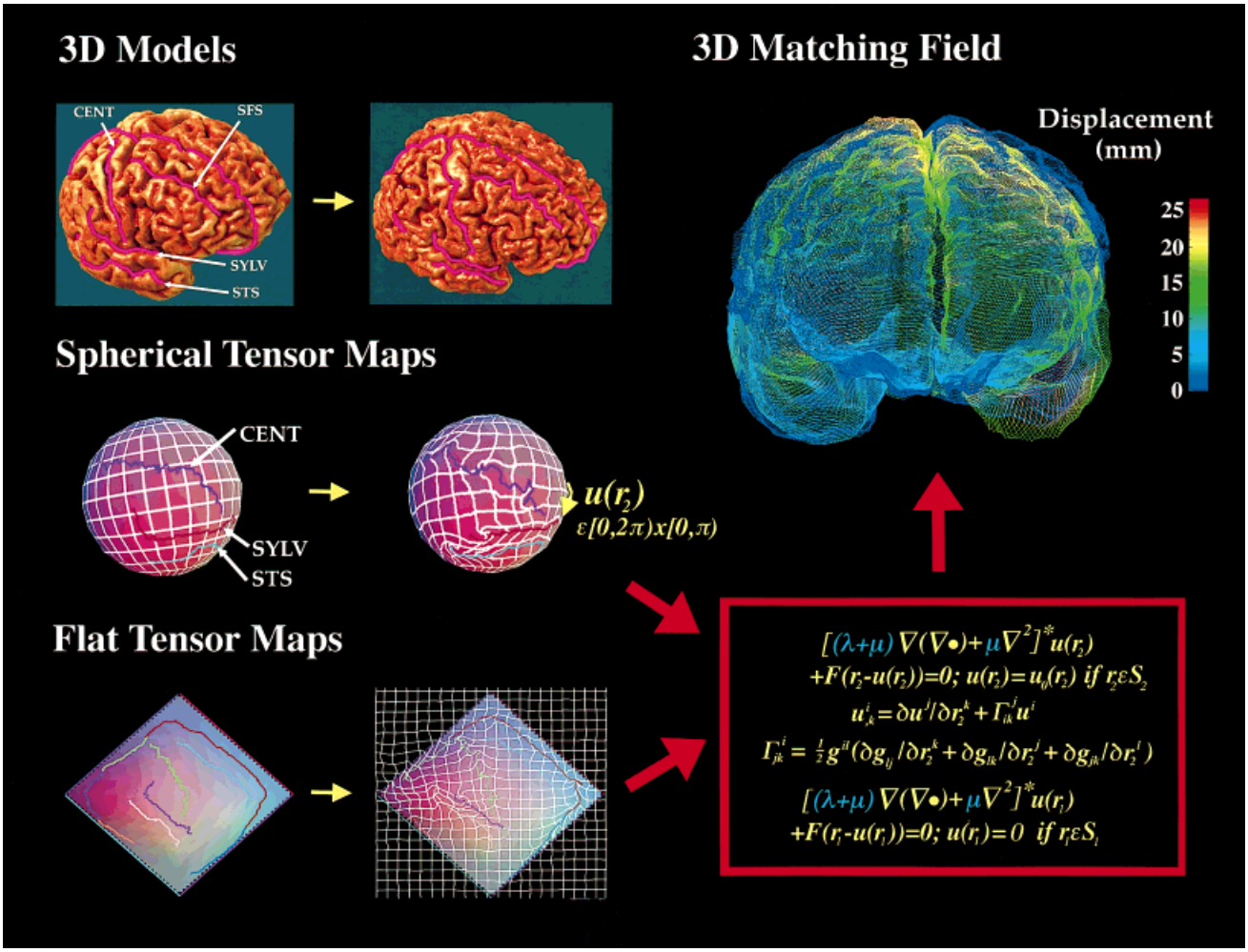

Figure 1.

Maps of the human cerebral cortex: flat, spherical, and tensor. Extreme differences in cortical patterns (3D models, top left) present challenges in brain mapping, because of the need to compare and integrate cortically derived brain maps from many subjects. Cortical geometry is compared by warping one subject's cortex onto another (top right). These warps can also transfer functional maps from one subject to another, or onto a common anatomic template for comparison. Matching cortical surfaces requires more than the matching of overall cortical geometry. Connected systems of curved sulcal landmarks, distributed over the cortical surface, must also be driven into correspondence with their counterparts in each target brain. Current approaches for deforming one cortex into the shape of another, typically simplify the problem by first representing cortical features on a 2D plane, sphere, or ellipsoid, where the matching procedure (i.e., finding $\mathbf{u}(\mathbf{r}_2)$, above) is performed. Here, active surface extraction of the cortex provides a continuous inverse mapping from the cortex of each subject to the spherical template used to extract it. Application of these inverse maps to connected networks of curved sulci in each subject transforms the problem into one of computing an angular flow vector field $\mathbf{u}(\mathbf{r}_2)$, in spherical coordinates that drives the network elements into register on the sphere (middle panel). The full mapping (top right) can be recovered in 3D space as a displacement vector field that drives cortical regions in one brain into precise registration with their counterparts in the other brain. Tensor maps (middle and lower left): Although these simple two-parameter surfaces can serve as proxies for the cortex, different amounts of local dilation and contraction (encoded in the metric tensor if the mapping, $g_{jk}(\mathbf{r})$) are required to transform the cortex into a simpler two-parameter surface. These variations complicate the direct application of 2D regularization equations for matching their features. A covariant tensor approach (red box) addresses this difficulty. The regularization operator L is replaced by its covariant form $L^{\ddagger}$, in which correction terms (Christoffel symbols, $\mathbf{\Gamma^i_{jk}}$) compensate for fluctuations in the metric tensor of the flattening procedure. This allows either flat or spherical maps to support cross-subject comparisons and registrations of cortical data by eliminating the confounding effects of metric distortions that necessarily occur in the flattening procedure.

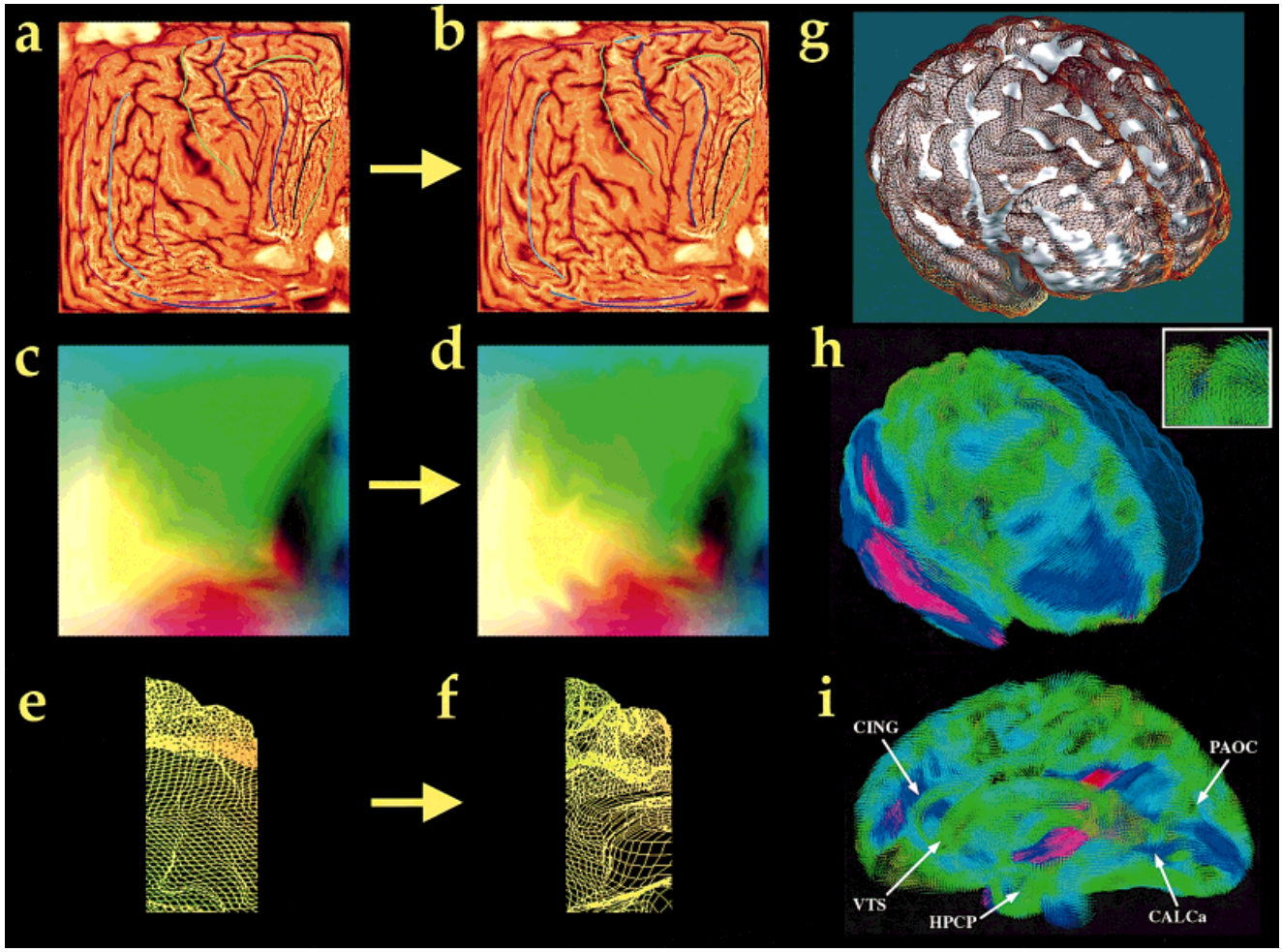

Figure 2.

Gyral pattern matching. **(a)** Flat cortical map for the left hemisphere of one subject, with the average cortical pattern for the group overlaid (colored lines). **(b)** Result of warping the individual's sulcal pattern into the average configuration for the group, using the covariant field equations (Appendix). The individual cortex (a) is reconfigured (b) to match the average set of cortical curves. The 3D cortical regions that map to these average locations are then recovered in each individual subject, as follows. A color code **(c)** representing 3D cortical point locations **(e)** in this subject is convected along with the flow that drives the sulcal pattern into the average configuration for the group **(d)**. Once this is done in all the subjects, points on each individual's cortex are recovered **(f)** that have the same relative location to the primary folding pattern in all subjects. Averaging of these corresponding points results in a crisp average cortex (see Fig. 3). Three-dimensional variability patterns across the cortex are also measured by driving individual cortical patterns into local correspondence with the average cortical model. Panel **(g)** shows how one subject's anatomy (brown surface mesh) deviates from the average cortex (white), after affine alignment of the individual data. In **(h),** the deformation vector field required to reconfigure the gyral pattern of the subject into the exact configuration of the average cortex. The transformation is shown as a flow field that takes the individual's anatomy onto the right hemisphere of the average cortex (blue surface mesh). The greatest deformation is required in temporal and parietal cortex (pink colors, large deformation). Details of the 3D vector deformation field (h, inset) show the local complexity of the mapping. Storage of these mappings allows quantification of local anatomic variability. **(i)** Continuum-mechanical mapping of a patient into the group average configuration. Instead of matching just the cortex, this figure shows the complex transformation required to match 84 surface models in a given patient, after affine alignment, into the configuration of an average surface set derived for the group. The effects of several anatomic surfaces driving the transformation are indicated, including the cingulate sulcus (CING), hippocampal surface (HPCP), superior ventricular horn (VTS), parieto-occipital sulcus, and the anterior calcarine fissure (CALCa). This surface-based vector field is extended to a full volumetric transformation field (0.1 billion degrees of freedom) [Thompson and Toga, 1996], which reconfigures the patient's anatomy into correspondence with the average configuration for the group. These transformation fields are stored and used to measure regional variability.

ate an *average* cortex. To do this, all 36 gyral curves for all subjects were first transferred to the spherical parameter space. Next, each curve was uniformly reparameterized to produce a regular curve of 100 points on the sphere whose corresponding 3D locations were uniformly spaced. A set of 36 average gyral curves for the group was created by vector averaging all point locations on each curve. This *average curve template* (*curves* in Fig. 2b) served as the target for alignment of individual cortical patterns [*cf.* Fischl et al., 1999]. Each individual cortical pattern was transformed into the configuration of the average curve template using a flow field within the spherical map (Fig. 2a,b). By carrying a color code (that indexes 3D locations) along with the vector flow that aligns each individual with the average folding pattern, information can be recovered at a particular location in the average folding pattern (Fig. 2d) specifying the 3D cortical points mapping each subject to the average. This produces a new coordinate grid on a given subject's cortex (Fig. 2f) in which particular grid-points appear in the same location across subjects relative to the mean gyral pattern. By averaging these 3D positions across subjects, an average 3D cortical model was constructed for the group (Fig. 2g). The resulting mapping is guaranteed to average together all points falling on the same cortical locations across the set of brains, and ensures that corresponding features are averaged together.

Cortical variability

By using the color code (Fig. 2d) to identify original cortical locations in 3D space (Fig. 2f), displacement fields were recovered mapping each patient into gyrus-by-gyrus correspondence with the average cortex (Fig. 2h). Anatomic variability was defined at each point on the average cortical surface as the root mean square (r.m.s.) magnitude of the 3D displacement vectors, assigned to each point, in the surface maps from individual to average [Thompson et al., 1996a,b, 1997]. This variability pattern was visualized as a color-coded map (Fig. 3d).

RESULTS

Cortical variability patterns

Overall, variability values rose sharply (Fig. 3d) from 4–5 mm in primary motor cortex to localized peaks of maximal variability in posterior perisylvian zones and superior frontal association cortex (12–14 mm). Primary sensory and motor areas showed a dramatic, localized invariance (2–5 mm), but variability rose sharply with the transition anteriorly from motor area 4 to prefrontal heteromodal association cortex. Intermediate variability values (6–10 mm) over the inferior prefrontal convexity fell sharply with the transition to archicortical orbitofrontal cortex, where the gyral pattern is highly conserved across subjects (2–5 mm variability). More laterally, the posterior frontal cortex, including territory occupied by Broca's area, displayed intermediate variability (6–10 mm). Temporal lobe variability rose from 2–3 mm in the depths of the Sylvian fissure to 14 mm at the posterior limit of the inferior temporal sulcus in both brain hemispheres, in the vicinity of area MT (Fig. 3d) [Watson et al., 1993], extending into the posterior heteromodal association cortex of the parietal lobe (12–14 mm).

Emerging patterns

After group averaging of anatomy, specific features of anatomy emerge that are not observed in individual anatomies due to their considerable variability (*q.v.*, Fig. 1). As shown in Figure 3 (*sagittal projection*), the marked anatomic asymmetry in posterior perisylvian cortex [Geschwind and Levitsky, 1968], actually extends rostrally into postcentral cortex, with the posterior bank of the postcentral gyrus thrust forward by 8–9 mm on the right compared to the left. The asymmetry also extends caudally across the lateral convexity into superior and inferior temporal cortex. The improved ability to localize asymmetry and encode its variability in a disease-specific atlas has encouraged us to develop a probabilistic atlas of the brain in schizophrenia [Narr et al., 1999]. Since relatively subtle asymmetries emerge clearly in a group atlas, population-based atlases may be advantageous for investigating hypothesized alterations in cortical organization or lateralization [Kikinis et al., 1994; *cf*. Csernansky et al., 1998].

AVERAGE IMAGE TEMPLATE CONSTRUCTION

The cortical transformations defined here also permit the construction of a disease-specific image template with the mean intensity and geometry for the AD population. By averaging geometric and intensity features separately [*cf*. Bookstein, 1997; Grenander and Miller, 1998], the resulting brain template has well-resolved cortical features in their mean anatomic location. To produce an average template for the group, nine brains were selected for whom additional anatomic surface models were created [Thompson et

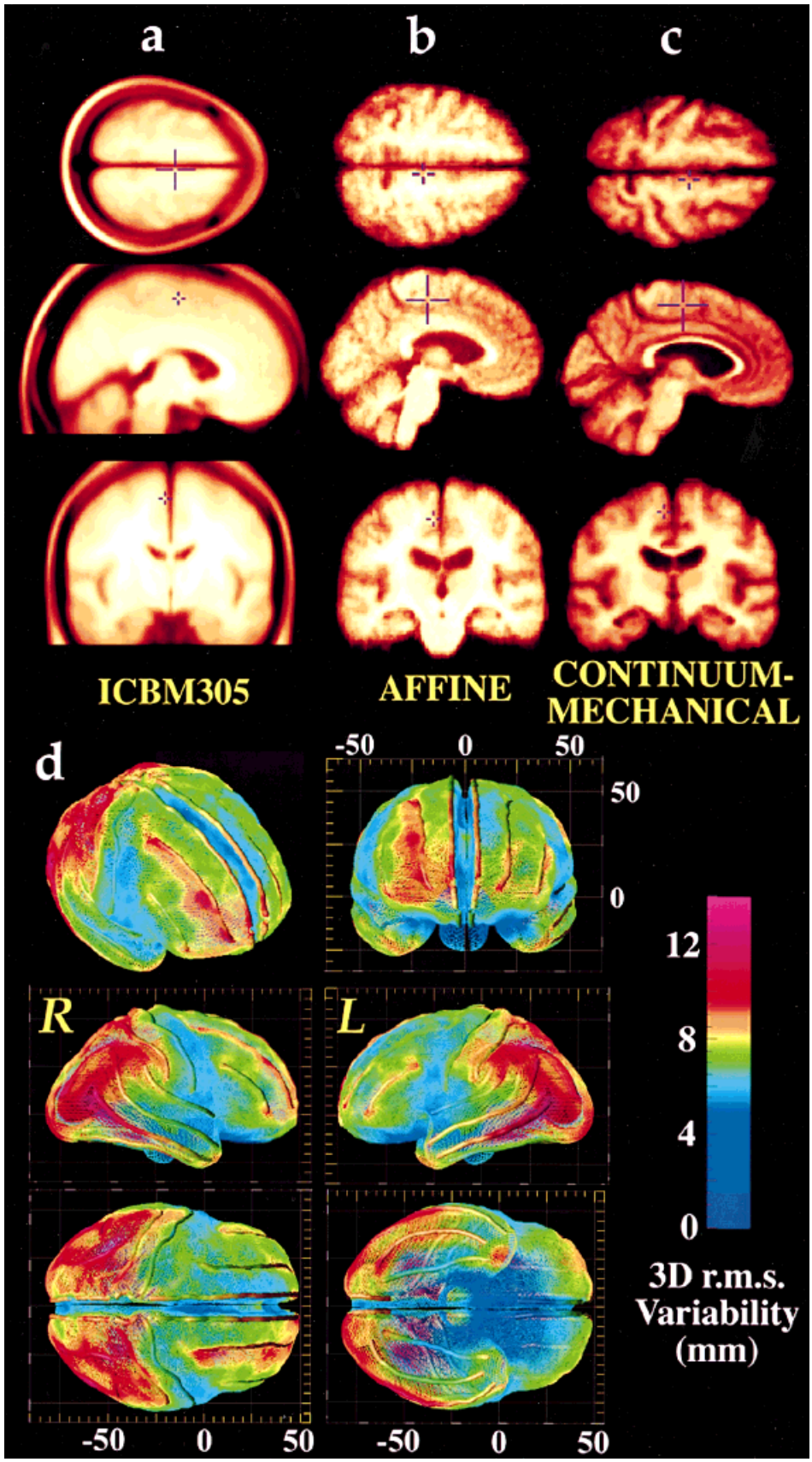

Figure 3.
Average brain templates and 3D cortical variability. Axial, sagittal, and coronal images are shown from a variety of population-based brain image templates. For comparison purposes, **(a)** shows a widely used average intensity dataset (ICBM305) based on 305 young normal subjects, created by the *International Consortium for Brain Mapping* [Evans et al., 1994]; by contrast, **(b)** and **(c)** are average brain templates created from high-resolution 3D MRI scans of Alzheimer's disease patients. (b) Affine brain template, constructed by averaging normalized MR intensities on a voxel-by-voxel basis data after automated affine registration. (c) Continuum-mechanical brain template, based on intensity averaging after continuum-mechanical transformation. By using spatial transformations of increasing complexity, each patient's anatomy can increasingly be reconfigured into the average anatomical configuration for the group. After intensity correction and normalization, the reconfigured scans are then averaged on a pixel-by-pixel basis to produce a group image template with the average geometry and average image intensity for the group. Anatomical features are highly resolved, even at the cortex (c). Transformations of extremely high spatial dimension are required to match cortical features with sufficient accuracy to resolve them after scans are averaged together. **(d)** The profile of variability across the cortex is shown ($N = 26$ subjects), after differences in brain orientation and size are removed by transforming individual data into Talairach stereotaxic space. The following views are shown: oblique frontal, frontal, right, left, top, bottom. Extreme variability in posterior perisylvian zones and superior frontal association cortex (12–14 mm; red colors) contrasts sharply with the comparative invariance of primary sensory, motor, and orbitofrontal cortex (2–5 mm, blue colors). Models are orthographically projected onto the Talairach stereotaxic grid to facilitate comparisons with activation data from functional imaging studies reported in this system [Fox et al., 1994].

al., 1998]. An initial image template for the group was constructed by (1) using automated linear transformations [Woods et al., 1993] to align the MRI data with a randomly selected image, (2) intensity-averaging the aligned scans, and then (3) recursively re-registering the scans to the resulting average affine image. The resulting average image was adjusted to have the mean affine shape for the group [Woods et al., 1998]. Images and surface models were then linearly aligned to this template, and an average surface set was created for the group [Thompson et al., 1997]. Displacement maps (Fig. 2h) driving the surface anatomy of each subject into correspondence with the average surface set were then extended to the full volume with a 3D warping algorithm based on surface-driven elasticity [Thompson and Toga, 1996, 1998]. These warping fields (Fig. 2h,i) reconfigured each subject's 3D image into the average anatomic configuration for the group. By averaging the reconfigured images (after intensity normalization), a crisp image template was created to represent the group (Fig. 3c). Note the better-resolved cortical features in the average images after high-dimensional cortical registration. If desired, this AD-specific atlas can retain the coordinate matrix of the Talairach system (with the AC at 0,0,0) while refining the gyral map of the Talairach atlas to encode the unique anatomy of the AD population. By explicitly computing matching fields that relate gyral patterns across subjects, a well-resolved and spatially consistent set of probabilistic anatomical models and average images can be generated to represent the average anatomy and its variation in a subpopulation.

CONCLUSION

Encoding patterns of anatomical variation in human populations present significant challenges. By describing an atlasing scheme that treats intensity and geometric variation separately [Bookstein, 1997; Gee et al., 1998; Grenander and Miller, 1998], it is possible to construct well-resolved image templates and probabilistic models of cortex that reflect the average anatomy of a group. Since the anatomy of a dementia population is poorly reflected by current imaging templates, substantially less distortion will be applied by mapping multimodality brain data into an atlas that reflects AD morphology [Mega et al., 1997; Thompson et al., 1998; Woods et al., 1999]. Incoming subjects deviate least from the mean template in terms of both image intensity and anatomy, so registration of their data to this template requires minimal image distortion.

Genetic analogy

As anatomical image databases increase in size and content and as brain image matching algorithms improve in speed and accuracy, deformation fields can be recovered that accurately map all images of a given type to a common digital template. This raises several interesting mathematical and practical issues. To use a genetic analogy, the template can be regarded as a probe screening a library, although here the library consists of brain images rather than DNA. The way in which the probe, or template, anneals to target molecules in a cDNA library depends on their individual degree of resemblance to the sequence of the probe itself. This matching criterion is formulated in the brain image matching context by defining a measure of affinity (such as mean squared intensity difference, plus a deformation energy), which is optimized by tuning the deformation field parameters. The matching energies that are optimized in a registration problem are akin to the annealing energies when a specially prepared probe screens a cDNA library. Since the deformation fields contain valuable information for pathology detection and deformation-based morphometry, the question arises as to what is the optimal probe or template to use. The accuracy of the deformation fields depends not only on the algorithm used, but also on the template to which individual scans are matched. Although there are characteristics that are clearly advantageous to have in a registration template (such as having a mean shape and good intensity contrast), these characteristics have rarely been investigated systematically. At the same time, well-resolved anatomical templates can be constructed for image registration, using a coarse-to-fine combination of automated polynomial [Woods et al., 1998] and anatomically driven continuum-mechanical [Thompson and Toga, 1996, 1998; Grenander and Miller, 1998] matching approaches. Interestingly, automated registration approaches were able to reduce anatomic variability to a greater degree if the specially prepared image template was used as a registration target [Thompson et al., 1999]. The continual refinement of anatomic templates is likely to be leveraged by algorithms for deformation-based morphometry in large image databases [Ashburner et al., 1998], for pathology detection based on encoded information on patterns of variability [Thompson et al., 1997], and by next-generation probabilistic atlases.

Probabilistic atlases that result from anatomical modeling and averaging are expandable and may be stratified into subpopulations according to clinical, demographic, or genetic criteria. Atlas data on ana-

tomic variability can also serve as Bayesian prior information to guide algorithms for automated image registration and labeling [Ashburner et al., 1998; Gee et al., 1998; Pitiot et al., 1999]. Conversely, variability mapping can be used systematically to evaluate how well different image registration approaches reduce regional anatomic variance [Thompson et al., 1999; Woods et al., 1999]. As well as disease-specific atlases reflecting brain structure in dementia and schizophrenia [Thompson et al., 1999; Narr et al., 1999], research is underway to build dynamic brain atlases that retain probabilistic information on temporal rates of growth and regressive processes during brain development and degeneration [Thompson et al., 1999]. Refinement of these atlas systems to support dynamic and disease-specific data should generate an exciting framework to investigate variations in brain structure and function in large human populations.

APPENDIX

Elastic Matching of Gyral Patterns using Flow Fields

Differences in cortical patterns between any pair of subjects can be determined by defining a flow field in the cortical parameter space (Fig. 1). A corresponding 3D displacement can be recovered between cortical models that matches a large network of sulcal features. On the sphere, the parameter shift function $\mathbf{u(r)}:\Omega \rightarrow \Omega$, is given by the solution $F_{pq}:\mathbf{r}\rightarrow\mathbf{r}\text{-}\mathbf{u}(\mathbf{r})$ to a curve-driven warp in the spherical parametric space $\Omega=[0,2\pi)\times[0,\pi)$ of the cortex [Thompson et al., 1996, 1998]. Briefly, for points $\mathbf{r}=(r,s)$ in the parameter space, a system of simultaneous partial differential equations can be written for the flow field $\mathbf{u}(\mathbf{r})$:

$$L(\mathbf{u}(\mathbf{r})) + \mathbf{F}(\mathbf{r} - \mathbf{u}(\mathbf{r})) = \mathbf{0},\ \forall\, \mathbf{r} \in \Omega,$$
$$\mathbf{u}(\mathbf{r}) = \mathbf{u}_0(\mathbf{r}),\ \forall\, \mathbf{r} \in M_0 \cup M_1. \quad (1)$$

Here M_0, M_1 are sets of points and (sulcal or gyral) curves where displacement vectors $\mathbf{u}(\mathbf{r}) = \mathbf{u_0}(\mathbf{r})$ matching corresponding anatomy across subjects are known. The flow behavior is modeled using equations derived from continuum mechanics, and these equations are governed by the Cauchy-Navier differential operator $L = \mu\nabla^2+(\lambda+\mu)\nabla(\nabla^T\bullet)$ with body force $\mathbf{F}$ [Thompson et al., 1996, 1998; Grenander and Miller, 1998]. In solving the governing equation matching sulcal networks across subjects, dependencies between the metric tensors of the surface parameterizations and the matching field are eliminated by using generalized coordinates and Christoffel symbols [Thompson and Toga, 1998]. Finally, the cortical transformation is recovered as a 3D mapping that drives one cortex onto another (Fig. 2e–i).

Flattening and distortion

Although planar (or spherical) maps serve as proxies for the cortex (Fig. 1), different amounts of local dilation and contraction are required to transform the cortex onto these simpler two-parameter surfaces. In the covariant tensor approach [Thompson and Toga, 1998], exact information on these metric alterations is encoded by the metric tensor of the mapping, $g_{\mathbf{jk}}(\mathbf{r})$. In the subsequent matching procedure, correction terms (Christoffel symbols, $\mathbf{\Gamma^i_{jk}}$) make the necessary adjustments for fluctuations in the metric tensor of the mapping procedure. Since metric distortions caused by mappings to spheres or planes can always be encoded as a metric tensor field, a covariant approach supports comparisons of cortical data using *either* flattened or spherical maps. In the partial differential equation formulation (1), we replace L by the covariant differential operator $L^{\ddagger}$. In $L^{\ddagger}$, all L's partial derivatives are replaced with covariant derivatives. These covariant derivatives are defined with respect to the metric tensor of the surface domain where calculations are performed. The covariant derivative of a (contravariant) vector field, $u^i(\mathbf{x})$, is defined as [Thompson and Toga, 1998]:

$$u^i{}_{,k} = \partial u^j/\partial x^k + \Gamma^j_{ik}u^i \quad (2)$$

where the $\mathbf{\Gamma^i_{jk}}$ are *Christoffel symbols of the second kind* [Einstein, 1914]. This expression involves not only the rate of change of the vector field itself, as we move along the cortical model, but also the rate of change of the local basis, which itself varies due to the intrinsic curvature of the cortex. On a surface with no intrinsic curvature, the extra terms (Christoffel symbols) vanish. The Christoffel symbols, expressed in terms of derivatives of components of the metric tensor $g_{jk}(\mathbf{x})$, are calculated directly from the cortical model:

$$\Gamma^i_{jk} = (1/2)g^{il}(\partial g_{lj}/\partial x^k + \partial g_{lk}/\partial x^j - \partial g_{jk}/\partial x^i). \quad (3)$$

Scalar, vector, and tensor quantities, in addition to the Christoffel symbols required to implement the diffusion operators on a curved manifold are evaluated by finite differences. These correction terms are then used in the solution of the Dirichlet problem [Joshi et al., 1995] for matching one cortex with another. Finally,

because 3D cortical positions are encoded in color on the spherical maps, the spherical transformation is recovered in 3D as a mapping that drives one cortex onto another. With this mathematical adjustment, we eliminate the confounding effects of metric distortions that necessarily occur during the mapping procedure and produce a cortical matching field that is independent of the auxiliary mappings (spherical or planar) used to extract it.

REFERENCES

Ashburner J, Friston K.1997. Multimodal image coregistration and partitioning — a unified framework. NeuroImage 6:209–217.

Ashburner J, Hutton C, Frackowiak R, Johnsrude I, Price C, Friston K.1998. Identifying global anatomical differences: deformation-based morphometry. Hum Brain Mapp 6:348–357.

Bookstein FL.1997. Landmark methods for forms without landmarks: morphometrics of group differences in outline shape. Med Image Analysis 1:225–243.

Cao J, Worsley KJ.1999. The geometry of the Hotelling's T-squared random field with applications to the detection of shape changes. Annals of Statistics (in press).

Christensen GE, Rabbitt RD, Miller MI. 1993. A deformable neuroanatomy textbook based on viscous fluid mechanics. 27th Ann. Conf. on Inf. Sciences and Systems, p 211–216.

Collins DL, Peters TM, Evans AC.1994. An automated 3D non-linear image deformation procedure for determination of gross morphometric variability in the human brain. Proc Visualization in Biomed. Comp (SPIE) 3:180–190.

Collins DL, Le Goualher G, Venugopal R, Caramanos A, Evans AC, Barillot C.1996. Cortical constraints for non-linear cortical registration. In: Höhne KH, Kikinis R, editors. Visualization in biomedical computing. Hamburg, Germany, Sept. 1996, Lecture notes in computer science. Berlin: Springer Verlag. p 307–316.

Cook MJ, Free SL, Fish DR, Shorvon SD, Straughan K, Stevens JM.1994. Analysis of cortical patterns. In: Shorvon SD, editor. Magnetic resonance scanning and epilepsy. New York: Plenum. p 263–274.

Courchesne E.1997. Brainstem,cerebellar and limbic neuroanatomical abnormalities in autism. Curr Opin Neurobiol 7:269–278.

Csernansky JG, Joshi S, Wang L, Haller JW, Gado M, Miller JP, Grenander U, Miller MI. 1998. Hippocampal morphometry in schizophrenia by high dimensional brain mapping. Proc Natl Acad Sci USA 95:11406–11411.

Davatzikos C. 1998. Mapping image data to stereotaxic spaces: applications to brain mapping. Hum Brain Mapp 6:334–338.

Dinov ID,Mega MS, Thompson PM, Lee L, Woods RP, Holmes CJ, Sumners DW, Toga AW. Analyzing functional brain images in a probabilistic atlas: a validation of sub-volume thresholding. J. Comp. Assist. Tomogr. (in press).

Drury HA, Van Essen DC. 1997. Analysis of functional specialization in human cerebral cortex using the Visible Man surfaced based atlas. Hum Brain Mapp 5:233–237.

Einstein A. 1914. Covariance properties of the field equations of the theory of gravitation based on the generalized theory of relativity, 29 May 1914, published as *Kovarianzeigenschaften der Feldgleichungen der auf die verallgemeinerte Relativitätstheorie gegründeten Gravitationstheorie*, Zeitschrift für Mathematik und Physik 63: 215–225.

Evans AC, Dai W, Collins DL, Neelin P, Marrett S.1991. Warping of a computerzied 3D atlas to match brain image volumes for quantitative neuroanatomical and functional analysis. SPIE Med Imaging 1445:236–247.

Evans AC, Collins DL, Neelin P, MacDonald D, Kamber M, Marrett TS. 1994. Three-dimensional correlative imaging: applications in human brain mapping. In: Thatcher RW, Hallett M, Zeffiro T, John ER, Huerta M, editors. Functional neuroimaging: technical foundations. p 145–162.

Filipek PA.1996. Brief report: neuroimaging in autism: the state of the science 1995. J Autism Dev Disord 26:211–215.

Fischl B, Sereno MI, Tootell RBH, Dale AM. 1999. High-resolution inter-subject averaging and a coordinate system for the cortical surface (in press).

Folstein MF, Folstein SE, McHugh PR.1975. "Mini mental state": a practical method of grading the cognitive state of patients for the clinician. J Psychiatry Res 12:189–198.

Fox PT, Mikiten S, Davis G, Lancaster JL. 1994. BrainMap: a database of human functional brain mapping. In: Thatcher RW, Hallett M, Zeffiro T, John ER, Huerta M, editors. Functional brain mapping: technical foundations. p 95–106.

Friedland RP, Luxenberg J. 1988. Neuroimaging and dementia. In: Theodore, WH, editor. Clinical neuroimaging: frontiers in clinical neuroscience, vol. 4. New York: Liss. p 139–163.

Gaser C, Kiebel S, Riehemann S, Volz H-P, Sauer H.1998. Statistical parametric mapping of structural changes in brain — application to schizophrenia research, poster #0718. 4th Int. Conf. on Functional Mapping of the Human Brain, Montreal.

Ge Y, Fitzpatrick JM, Kessler RM, Jeske-Janicka M.1995. Intersubject brain image registration using both cortical and subcortical landmarks. SPIE Image Proc 2434:81–95.

Gee JC, Bajcsy RK.1998. Elastic matching: continuum-mechanical and probabilistic analysis. In: Toga AW, editor. Brain warping. San Diego: Academic Press.

Giedd JN, Castellanos FX, Casey BJ, Kozuch P, King AC, Hamburger SD, Rapaport JL.1994. Quantitative morphology of the corpus callosum in attention deficit hyperactivity disorder. Am J Psychiatry 151: 665–669.

Grenander U, Miller MI. 1998. Computational anatomy: an emerging discipline. Technical Report, Dept. of Mathematics, Brown University.

Joshi SC, Miller MI, Christensen GE, Banerjee A, Coogan TA, Grenander U. 1995. Hierarchical brain mapping via a generalized Dirichlet solution for mapping brain manifolds, Vision geometry IV. Proc SPIE Conference on Optical Science, Engineering and Instrumentation, San Diego, Aug 2573:278–289.

Kennedy DN, Lange N, Makris N, Bates J, Meyer J, Caviness VS Jr. 1998. Gyri of the human neocortex: an MRI-based analysis of volume and variance. Cereb Cortex 8:372–384.

Kikinis R, Shenton ME, Gerig G, Hokama H, Haimson J, O'Donnell BF, Wible CG, McCarley RW, Jolesz FA.1994. Temporal lobe sulco-gyral pattern anomalies in schizophrenia: an in vivo MR three-dimensional surface rendering study. Neurosci Lett 182: 7–12.

Labbe C, Froment JC, Kennedy A, Ashburner J, Cinotti L.1996. Positron emission tomography metabolic data corrected for cortical atrophy using magnetic resonance imaging. Alzheimer Dis Assoc Disord 10:141–170.

MacDonald D.1998. A method for identifying geometrically simple surfaces from three dimensional images, PhD thesis, McGill Univ, Canada.

Mazziotta JC, Toga AW, Evans AC, Fox P, Lancaster J.1995. A probabilistic atlas of the human brain: theory and rationale for its development. NeuroImage 2:89–101.

Mega MS, Chen S, Thompson PM, Woods RP, Karaca TJ, Tiwari A, Vinters H, Small GW, Toga AW. 1997. Mapping pathology to metabolism: coregistration of stained whole brain section to PET in Alzheimer's disease. NeuroImage 5:147–153.

Narr KL, Sharma T, Moussai J, Zoumalan CI, Cannestra AF, Thompson PM, Toga AW. 1999. 3D maps of cortical surface variability and sulcal asymmetries in schizophrenic and normal populations. 5th International Conference on Functional Mapping of the Human Brain, Dusseldorf, Germany.

Ono M, Kubik S, Abernathey CD.1990. Atlas of the cerebral sulci. Stuttgart: Thieme.

Paus T, Tomaioulo F, Otaky N, MacDonald D, Petrides M, Atlas J, Morris R, Evans AC. 1996. Human cingulate and paracingulate sulci: pattern, variability, asymmetry and probabilistic map. Cereb Cortex 6:207–214.

Pitiot A, Thompson PM, Toga AW.1999. Spatially and temporally adaptive elastic template matching. IEEE Trans on Pattern Anal and Machine Intelligence (in press).

Roland PE, Zilles K.1994. Brain atlases—a new research tool. Trends in Neurosci 17:458–467.

Rizzo G, Gilardi MC, Prinster A, Grassi F, Scotti G, Cerutti S, Fazio F. 1995. An elastic computerized brain atlas for the analysis of clinical PET/SPET data. Eur J Nucl Med 22:1313–1318.

Sandor SR, Leahy RM. 1995. Towards automated labeling of the cerebral cortex using a deformable atlas. In: Bizais Y, Barillot C, Di Paola R, editors. Info Proc in Med Imag June 127–138.

Seitz RJ, Bohm C, Greitz T, Roland PE, Eriksson L, Blomqvist G, Rosenqvist G, Nordell B.1990. Accuracy and precision of the computerized brain atlas programme for localization and quantification in positron emission tomography. J Cereb Blood Flow Metab 10:443–457.

Sereno MI, Dale AM, Liu A, Tootell RBH.1996. A surface-based coordinate system for a canonical cortex. Proc 2nd Int. Conf Hum Brain Mapping, Boston. Neuroimage 3:S252.

Sled JG, Zijdenbos AP, Evans AC.1998. A non-parametric method for automatic correction of intensity non-uniformity in MRI data. IEEE Trans on Med Imaging, vol. 17.

Sobire G, Goutieres F, Tardieu M, Landrieu P, Aicardi J.1995. Extensive macrogyri or no visible gyri: distinct clinical, electroencephalographic, and genetic features according to different imaging patterns. Neurology 45:1105–1111.

Steinmetz H, Furst G, Freund H-J. 1990. Variation of perisylvian and calcarine anatomic landmarks within stereotaxic proportional coordinates. Am J Neuroradiol 11:1123–1130.

Talairach J, Tournoux P. 1988. Co-planar stereotaxic atlas of the human brain. New York: Thieme.

Thirion J-P, Prima S, Subsol S.1998. Statistical analysis of dissymmetry in volumetric medical images. Med Image Analysis (in press).

Thompson PM, Schwartz C, Toga AW.1996a. High-resolution random mesh algorithms for creating a probabilistic 3D surface atlas of the human brain. NeuroImage 3:19–34.

Thompson PM, Schwartz C, Lin RT, Khan AA, Toga AW. 1996b. 3D statistical analysis of sulcal variability in the human brain. J Neurosci 16:4261–4274.

Thompson PM, Toga AW. 1996c. A surface-based technique for warping 3-dimensional images of the brain. IEEE Trans on Med Imaging 15:1–16.

Thompson PM, MacDonald D, Mega MS, Holmes CJ, Evans AC, Toga AW.1997a. Detection and mapping of abnormal brain structure with a probabilistic atlas of cortical surfaces. J Comp Assist Tomogr 21:567–581.

Thompson PM, Toga AW.1997b. Detection, visualization and animation of abnormal anatomic structure with a deformable probabilistic brain atlas based on random vector field transformations. Med Image Analysis 1: 271–294; paper, with video sequences on CD-ROM with journal issue, November 1997.

Thompson PM, Moussai J, Khan AA, Zohoori S, Goldkorn A, Mega MS, Small GW, Cummings JL, Toga AW. 1998. Cortical variability and asymmetry in normal aging and Alzheimer's disease. Cereb Cortex 8:492–509.

Thompson PM, Toga AW.1998. Anatomically driven strategies for high-dimensional brain image warping and pathology detection. In:Toga AW, editor. Brain warping. San Diego: Academic Press. p 311–336.

Thompson PM, Narr KL, Blanton RE, Toga AW.1999. Mapping structural alterations of the corpus callosum during brain development and degeneration. In: Iacoboni M, Zaidel E, editors. The Corpus Callosum. New York: Academic Press.

Thompson PM, Mega MS, Woods RP, Blanton RE, Moussai J, Zoumalan CI, Aron J, Cummings JL, Toga AW. 1999. A probabilistic atlas of the human brain in Alzheimer's disease (in press).

Toga AW. 1998. Brain warping. San Diego: Academic Press.

Toga AW, Thompson PM. 1999. Multimodal brain atlases. In: Wong S, editor. Advances in biomedical image databases. New York: Academic Press.

Van Essen DC, Maunsell JHR.1980. Two-dimensional maps of the cerebral cortex. J Comp Neurol 191:255–281.

Watson JDG, Myers R, Frackowiak RSJ, Hajnal JV, Woods RP, Mazziotta JC, Shipp S, Zeki S. 1993. Area V5 of the human brain: evidence from a combined study using positron emission tomography and magnetic resonance imaging. Cereb Cortex 3:79–94.

Wells WM, Viola P, Atsumi H, Nakajima S, Kikinis R. 1997. Multimodal volume registration by maximization of mutual information. Med Image Analysis 1:35–51.

Woods RP, Cherry SR, Mazziotta JC.1992. Rapid automated algorithm for aligning and reslicing PET images. J Comp Assist Tomogr 16:620–633.

Woods RP, Mazziotta JC, Cherry SR. 1993. MRI-PET registration with automated algorithm. J Comp Assist Tomogr 17:536–546.

Woods RP, Grafton ST, Watson JDG, Sicotte NL, Mazziotta JC. Automated image registration: II. Intersubject validation of linear and nonlinear models. J Comp Assist Tomogr 22.

Zijdenbos AP, Dawant BM.1994. Brain segmentation and white matter lesion detection in MR images. Crit Rev Biomed Eng 22:401–465.